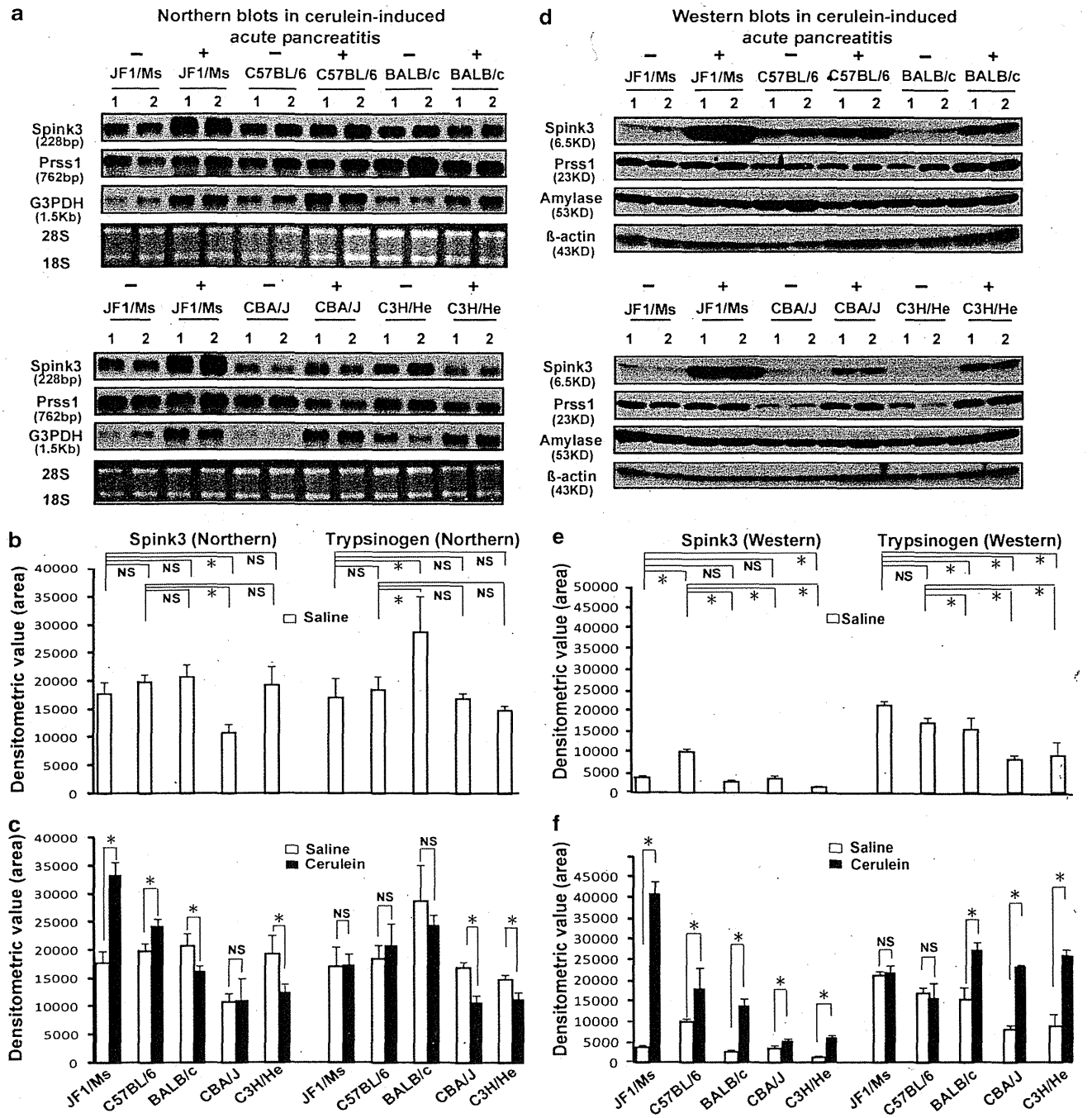

Figure 3 Northern and western blots analyses on Spink3, Prss1, and amylase expressions in cerulein-induced acute pancreatitis. (**a**) Northern blot analysis; 18S and 28S were used as loading controls because G3PDH expression was induced by cerulein treatment. The same JF1 samples were arranged in the first four lanes of northern blots. (**b**) Densitometric analysis for Spink3 and Prss1 expressions without cerulein induction in northern blot. (**c**) Densitometric analysis for Spink3 and Prss1 expressions with cerulein induction in northern blot. (**d**) Western blot analysis. *β*-actin was used as a loading control. The same JF1 samples were arranged in the first four lanes of western blots. (**e**) Densitometric analysis for Spink3 and Prss1 expressions after cerulein induction in western blot. (**f**) Densitometric analysis for Spink3 and Prss1 expressions with cerulein induction in western blot. Unfilled bars represent untreated strains of mice, whereas black bars indicate the treated strains. '−': saline treatment. '+': cerulein treatment. *$P<0.05$. NS: no significance.

Levels of Prss1 mRNA in JF1 and C57BL/6 strains were lower than those in other strains under a normal diet (Figure 5a and b). After CDE diet, levels of Prss1 mRNA were decreased in C57BL/6, BALB/c, CBA/J, and C3H/HeJ mice (Figure 4a and c). Protein expression for Spink3 and Prss1 was examined by western blot analyses. Under normal diet, the levels of Spink3 were again higher in JF1 and C57BL/6J than those in other three strains (Figure 4d and e). After CDE

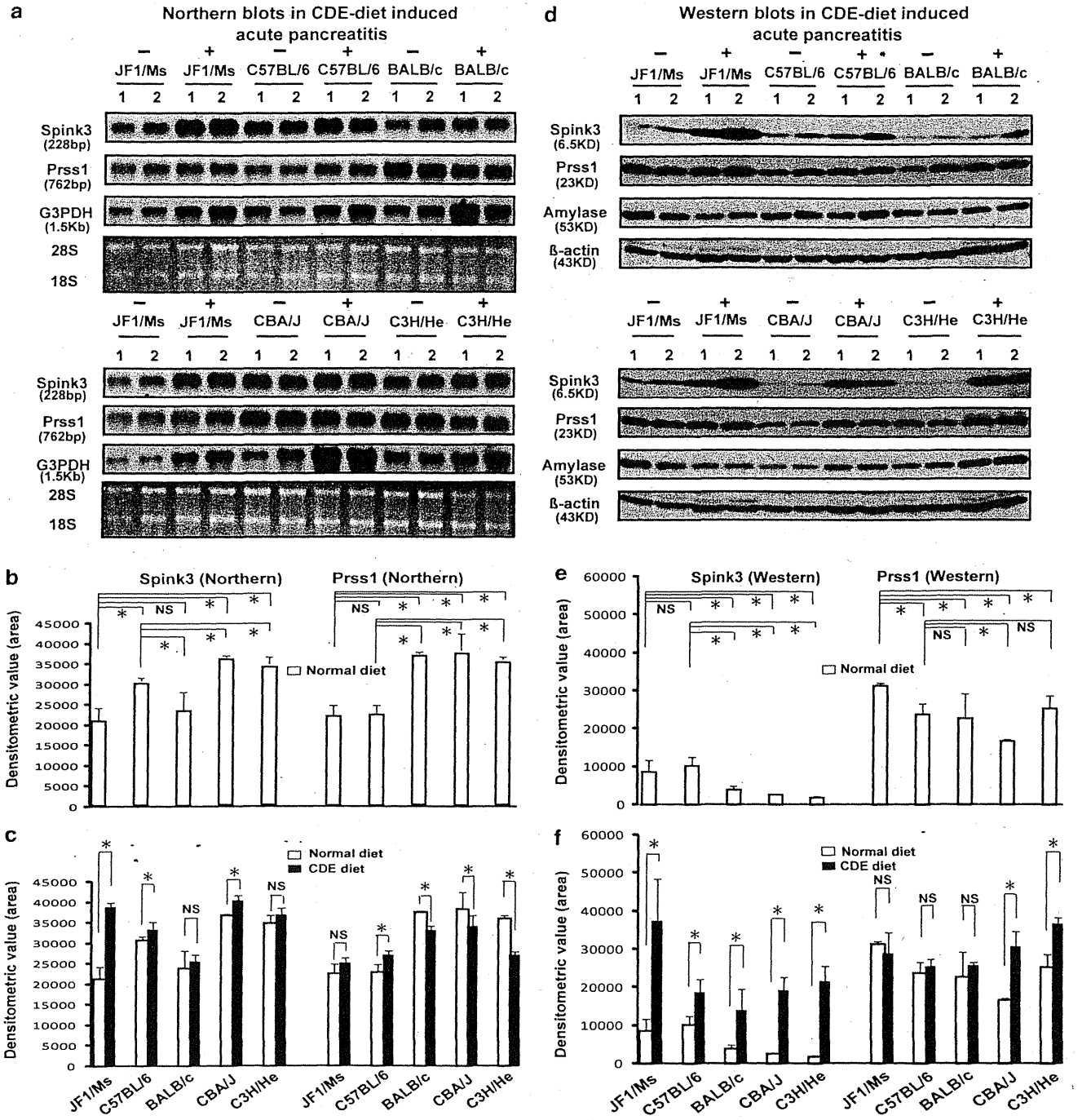

Figure 4 Northern and western blot analyses on Spink3, Prss1, and amylase expressions in CDE diet-induced acute pancreatitis. (**a**) Northern blot analysis; 18S and 28S were used as loading controls because G3PDH expression was induced by cerulein treatment. The same JF1 samples were arranged in the first four lanes of northern blots. (**b**) Densitometric analysis for Spink3 and Prss1 expressions without CDE diet in northern blot. (**c**) Densitometric analysis for Spink3 and Prss1 expressions with CDE diet in northern blot. (**d**) Western blot analysis. β-actin was used as a loading control. The same JF1 samples were arranged in the first four lanes of western blots. (**e**) Densitometric analysis for Spink3 and Prss1 expressions without CDE diet in western blot. (**f**) Densitometric analysis for Spink3 and Prss1 expressions with CDE diet in western blot. Unfilled bars represent untreated strains of mice, whereas black bars indicate the treated strains. $^*P<0.05$. NS: no significance.

diet, Spink3 expression increased significantly in JF1, but moderately in other strains (Figure 4d and f).

The level of Prss1 protein expression was lower in CBA/J than those in other four strains without CDE diet (Figure 4d and e). With CDE diet, Prss1 expression increased significantly in CBA/J and C3H/HeJ, whereas expression remained unchanged in JF1, C57BL/6J, and BALB/c mice (Figure 4d and f). These results also suggest that the induction levels of Spink3 and Prss1 are negatively and positively related to susceptibility of CDE-induced pancreatitis, respectively.

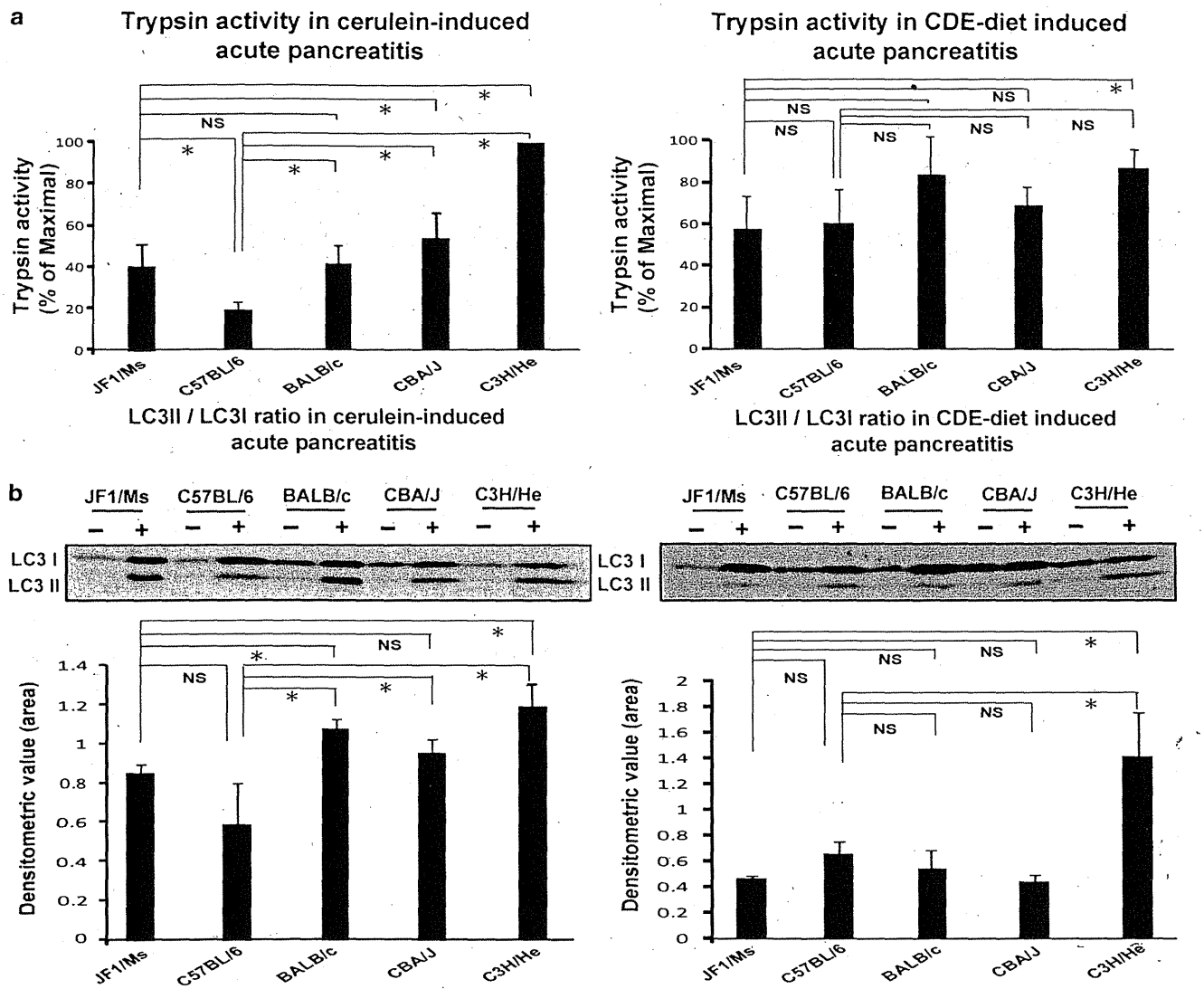

Figure 5 Trypsin activity and LC3-II expression. (**a**) Trypsin activity in cerulein-induced and CDE-diet-induced acute pancreatitis. Trypsin activity coincided with protein expression level of Prss1. (**b**) LC3-II/LC3-I ratio in cerulein-induced and CDE diet-induced acute pancreatitis. LC3-II levels were inversely related to Spink3 levels when treated with cerulein, suggesting the function of Spink3 as an inhibitor of autophagy.

Trypsin Activity

As activation or extent of trypsinogen to trypsin during initiation of acute pancreatitis is associated with the severity of acinar cell injury, we examined the trypsin activity level within pancreatic tissue homogenates among five mouse strains. The highest activity was shown in C3H/HeJ, followed by CBA/J, BALB/c, JF1, whereas C57BL/6J displayed the lowest value in cerulein-induced pacreatitis (Figure 5a, left panel). In CDE diet, trypsin activity level was significantly higher in C3H/HeJ than those in other strains (Figure 5a, right panel). Not surprisingly, the variation of trypsin activity was consistent with the expression pattern of trypsinogen among the five mouse strains.

Expression of LC3, an Autophagic Indicator

To approve that Spink3 functions also as a suppressor of autophagy, we checked in the five mouse strains the expression level of microtubule-associated protein 1 LC3. As LC3-I is converted into LC3-II during autophagosome formation, we determined the LC3-II/LC3-I ratio by densitometric analysis. As shown in Figure 5b, the ratio was higher in C3H/HeJ, BALB/c, and CBA/J than that in JF1 and C57BL/6J when treated with cerulein, showing that the mouse strain with higher Spink3 expression possessed low level of LC3-II, meaning less severe degree of autophagy.

Nucleotide Sequences of Prss1 and Spink3 cDNAs

To examine whether there was any nucleotide changes in coding regions of the *Prss1* and *Spink3* genes, we sequenced cDNA of these two genes isolated from all five strains. Nucleotide sequences of *Prss1* and *Spink3* cDNAs were exactly the same in four strains of mice: C57BL/6J, CBA/J, BALB/c, and C3H/HeJ. In contrast, in the 807 bp of the Prss1

Table 1 Single-nucleotide polymorphisms in JF1 cDNA *vs* B6

Prss1 (807 bp)			Spink3 (284 bp)		
Position	Nucleotide change	Amino-acid change	Position	Nucleotide change	Amino-acid change
Exon 1	15G>C	No	Exon 3	192G>A	No
Exon 3	342A>T	No	Exon 3	198C>T	No
Exon 4	516G>A	No	Exon 4	279A>G	No
Exon 4	519T>C	No			
Exon 4	568G>A	E190K			

JF1, Japanese Fancy Mouse 1. E190A, substitution of the glutamic acid (E) at amino-acid position 190 with lysine (K).

cDNA sequence of JF1 mice, five nucleotide changes were found (Table 1). However, only the alteration, G to A at position 568, resulted in substitution of glutamic acid with lysine at amino-acid position 190 (Table 1). On the other hand, three nucleotide changes were found within the 284 bp region of Spink3 cDNA of JF1 mice without an amino-acid substitution (Table 1).

Nucleotide Sequences of 3 kb Upstream Regions of Spink3 and Prss1 Genes

As expression patterns of Spink3 and Prss1 differed among mouse strains, we sequenced the approximately 3 kb promoter regions of Spink3 and Prss1 genes. We chose JF1 and C3H/HeJ as representatives of resistant and susceptible mouse strains, respectively. As the most conserved binding sites for transcription factors in pancreas-specific genes reside within the 1 kb upstream region, we focused on the 3 kb upstream regions of both Spink3 and Prss1 genes in this study. All of the sequence data were aligned and compared with the corresponding public database for C57BL/6J mice. For the upstream nucleotide sequence of the Spink3 gene, eight nucleotide changes (8/3000 = 0.27%) were found in C3H/HeJ *vs* C57BL/6J, whereas 92 nucleotide changes (92/3000 = 3.07%) appeared in JF1 *vs* C57BL/6J mice, representing a huge difference in the 3 kb upstream of the transcription start site in JF1 mice (Supplementary Figure 2). Notably, almost half of nucleotide changes[30] were found within the 1 kb upstream region in JF1 (Supplementary Figure 2). Several conserved motifs for transcription factors[31–36] were found in the 3 kb upstream regions of Spink3 genes as summarized in Supplementary Figure 2. Interestingly, an additional 10 bp was found between −372 and −381 in JF1 mice, although a conserved motif has not been reported around this region.

With respect to the Prss1 gene, 46 (46/3000 = 1.53%) or 39 (39/3000 = 1.30%) nucleotide changes were identified in C3H/He or JF1 strains against C57BL/6J mice, respectively (Supplementary Figure 3). However, the region between −3000 and −2300 bp of C57BL/6J was the same as that of JF1, but not of C3H. On the other hand, the region between −2300 and −1 bp of C57BL/6J mice was similar to that of C3H mice. Three binding sites were found in the 1 kb upstream region of the Prss1 gene[31,37] (Supplementary Figure 3). All these sequences are identical in all strains except one nucleotide change at −192 of the binding site (ATCACCTGCT) for nuclear protein in JF1 mice.

DISCUSSION

In this study, we showed strain differences using two models of experimental acute pancreatitis and identified a negative and positive relationship regarding the expression levels of Spink3 and Prss1, respectively, in the susceptibility to experimental acute pancreatitis. In addition, we showed that sequence differences in the promoter region of the Spink3 gene was significant between JF1 and other laboratory mouse strains, suggesting that differences in gene regulation are connected to a susceptibility to induced acute pancreatitis.

Pathologically, there were qualitative differences between cerulein- and CDE diet-induced pancreatitis in addition to the severity of pancreatitis. In the CDE diet model, much more hemorrhagic legions were noticed, as has been reported before.[28] This difference may be caused by different induction mechanisms in the early stages of acute pancreatitis. Cerulein is a cholecystokinin analog that can stimulate pancreatic acinar cells to secrete digestive enzymes. In supramaximal stimulation by cerulein, secretory activity increases dramatically, but membrane recruitment is insufficient for a strong demand of zymogen granule membrane, resulting in an inhibition of exocytosis at the luminal plasma membrane. On the other hand, a more likely target of ethionine is phospholipid metabolism of membranes that are involved in the processes of intracellular transport and secretion of pancreatic enzymes. Feeding a choline-deficient diet potentiated the activity of ethionine, because a choline-deficient diet also induced changes in membrane phospholipids of cellular organelles.[38–40] Although the detailed mechanism for hemorrhagic lesions remains unclear, destruction of the elastic tissue of the intrapancreatic vessels may also occur in such a situation.

In two experimental models, we observed similar strain differences in disease susceptibility, which were most severe in C3H/HeJ and CBA/J strains, moderate in BALB/c mice,

and mildest in C57BL/6J and JF1 strains. In human beings, a relationship between the PRSS1 gene mutations and the onset of pancreatitis has been established by many investigations.[21,30,41,42] Thus, it is possible that differences in primary structure or expression of the Prss1 gene are responsible for strain differences. Although we found one single-nucleotide polymorphism (SNP) in exon 4 that resulted in substitution of glutamic acid with lysine at amino-acid position 190 in JF1 mice, this mutation was not observed in the PRSS1 gene of human patients, suggesting that the coding region of the Prss1 gene is not related to the susceptibility to pancreatitis among these strains.

Interestingly, Prss1 protein expression was obviously increased in BALB/c, CBA/J, and C3H/HeJ mice, but not in JF1 and C57BL/6J mice with cerulein treatment. This high Prss1 expression coincided with a high trypsin activity. Many nucleotide changes found in the 3 kb upstream region of the Prss1 gene among C57BL/6J, C3H/HeJ, and JF1 strains may be responsible for different expression level.

Differences in the primary structure or expression of the Spink3 gene may also be involved in susceptibility to the development of pancreatitis. However, we could not find any SNPs with an amino-acid substitution between JF1 and other strains of mice. Thus, the coding region of the Spink3 gene was not related to pancreatitis susceptibility. Meaningfully, we found a significantly higher expression of Spink3 in JF1 and C57BL/6J mice under normal feeding (Figure 3a and b). Furthermore, Spink3 expression was strongly augmented in JF1 mice with cerulein treatment. This high Spink3 expression was associated with low level of LC3-II expression, implying the function of Spink3 as an inhibitor of autophagy. As shown in Supplementary Figure 2, we found significant nucleotide changes in the 3 kb upstream region of the Spink3 gene of JF1 mice. It is of interest that an additional 10 bp was inserted between −372 and −381 region in JF1 mice, although a conserved motif has not been reported around this region. Therefore, this region might be involved in the regulation of gene expression under cerulein stimulation. Taking these into account, the mechanisms by which Prss1 and Spink3 might be influencing the susceptibility are proposed here in a molecular model shown in Figure 6. In resistant strains, increased Spink3 expression caused by cerulein or CDE diet suppresses autophagy, leading to reduced activation of trypsinogen. In addition, Spink3 can bind to trypsin to inhibit its activity directly. Thus, both enhanced Spink3 and low Prss1 expression result in reduced trypsin activity, leading to less severe acute pancreatitis. In susceptible strains, low level of Spink3 expression results in enhanced autophagy, causing the conversion of trypsinogen to trypsin, and in low-level inhibition of trypsin. Thus, both high Prss1 and low Spink3 expressions result in increased trypsin activity, leading to more severe acute pancreatitis.

After activation of trypsinogen, inflammation is eventually induced in both models. Therefore, different responses in inflammatory factors, such as NF-κB, TNF-α, IL-1,

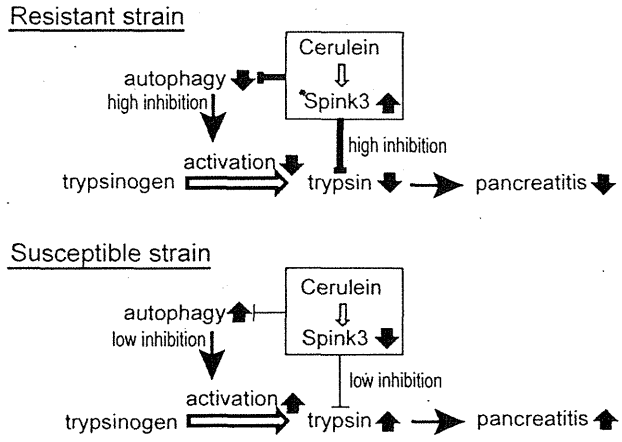

Figure 6 Proposed model for the function of Prss1 and/or Spink3 on susceptibility of acute pancreatitis. In resistant strains, increased Spink3 expression caused by cerulein suppresses autophagy, and trypsin activity, leading to less severe acute pancreatitis. In susceptible strains, low expression of Spink3 and high expression of Prss1 result in enhanced autophagy, causing the conversion of trypsinogen to trypsin and in low-level inhibition of trypsin, thus leading to more severe acute pancreatitis.

Heat Shock Protein, NO, or TLR4, among strains may be involved in pancreatitis susceptibility. Actually, inflammatory responses are different from one strain to another and a given strain can have variable inflammatory responses from one form of damage to another. For example, inbred mice varied significantly in their susceptibility to cigarette smoke-induced emphysema.[43,44] Further studies will be required to analyze genetic mechanisms for differences in inflammatory responses.

Advances in molecular physiology indicate the mouse to be an ideal investigative model to determine genomic variants that affect susceptibility to disease. This model offers the advantage of studying a large number of genetically identical animals under controlled conditions. Animal studies complement human studies by introducing an experimental control and the opportunity to pursue functional genomics and expression studies at the level of organs, tissues, or cells. Molecular mechanisms for disease resistance/susceptibility may differ among strains, and the JF1 strain may give a unique opportunity to examine such mechanisms that may not be found in other laboratory mouse strains.

Supplementary Information accompanies the paper on the Laboratory Investigation website (http://www.laboratoryinvestigation.org)

ACKNOWLEDGEMENTS

We herein sincerely appreciate the excellent work on the tissue sectioning preparation by Mrs Michiyo Nakata and Ms Yumi Otake. We also thank the Riken BioResource Center, Tsukuba, Japan for supplying JF1 mice. This work was supported in part by KAKENHI (Grant-in-Aid for Scientific Research) in Priority Areas 'Integrative Research Toward the Conquest of Cancer' (17012018) from the Ministry of Education, Culture, Sports, Science, and Technology, a Grant-in-Aid for Scientific Research (S) (21220010) and a Grant-in-Aid for Young Scientists (B) (18790968) from the Japan Society for the Promotion of Science (JSPS) of Japan.

Exp. Anim. 59(4), 421–429, 2010

—Original—

Chronic Pancreatitis in Mice by Treatment with Choline-Deficient Ethionine-Supplemented Diet

Satoshi IDA[1,2], Masaki OHMURAYA[1,3], Masahiko HIROTA[4], Nobuyuki OZAKI[2], Sayaka HIRAMATSU[1], Hitoshi UEHARA[1], Hiroshi TAKAMORI[2], Kimi ARAKI[1], Hideo BABA[2], and Ken-ichi YAMAMURA[1]

[1]*Insitute of Resource Development and Analysis, Kumamoto University, Kumamoto 860-0811, Japan,* [2]*Department of Gastroenterological Surgery, Kumamoto University Graduate School of Medical Sciences, Kumamoto University, Kumamoto 860-8556, Japan,* [3]*Priority Organization for Innovation and Excellence, Kumamoto University, Kumamoto 860-0811, Japan, and* [4]*Department of Surgery, Kumamoto Regional Medical Center, Kumamoto 860-0811, Japan*

Abstract: Although chronic pancreatitis is a risk factor for pancreatic ductal adenocarcinoma (PDA), the relationship between chronic pancreatitis and PDA remains obscure. A critical obstacle to understanding the role of chronic pancreatitis is the lack of animal models. To develop one such model, mice were fed long-term with a choline deficient ethionine-supplemented (CDE) diet. Histological evaluation revealed that chronic pancreatitis, characterized by acinar atrophy, fibrosis and well-developed tubular complexes (TCs), was observed after 24 weeks of CDE diet treatment. Furthermore, expression of epidermal growth factor receptor (EGFR) and its ligands; serine protease inhibitor Kazal type 3 (Spink3) and transforming growth factor α (TGF α) and activation of K-Ras (GTP-Ras formation), which are frequently observed in human PDA, were indeed observed in parallel with TCs formation. Neoplastic lesions were not found after 54 weeks of treatment, suggesting that a continuation of CDE diet or another insult is required for the development of PDA.

Key words: CDE diet, chronic pancreatitis, EGFR, Spink3, tubular complex

Introduction

Several recent reports have shown that chronic pancreatitis is a risk factor for pancreatic ductal adenocarcinoma (PDA) [25, 27]. This was clearly demonstrated in cases of hereditary chronic pancreatitis [26]. The incidence of pancreatic cancer in such patients increased 53 times more than that of the control [26]. However, information regarding the mechanisms behind the development of pancreatic carcinoma in the setting of chronic pancreatitis is scarce, particularly with respect to early molecular events. Concerning the molecular events in pancreatic adenocarcinoma and dysplasias, there are evidences for overexpression of epidermal growth factor receptor (EGFR) [32] and enhanced autocrine epidermal growth factor (EGF)-family signaling [4, 13, 19, 33, 38]. Consistent with the existence of such an autocrine loop, pancreatic adenocarcinomas overexpress EGF-family ligands, such as transforming growth factor α (TGF α) and EGF [13, 19]. EGFR and human

(Received 17 November 2009 / Accepted 3 January 2010)

Address corresponding: K. Yamamura, Division of Developmental Genetics, Institute of Molecular Embryology and Genetics, Kumamoto University, Kumamoto 860-0811, Japan

epidermal growth factor receptor 2 (HER2) induction also occurs in low-grade pancreatic intraepithelial neoplasms (PanINs), indicating that autocrine EGF family signaling is operative in the early stages of a pancreatic neoplasm [10]. However, it is not known whether such molecular events start during the onset of pancreatic carcinoma or chronic pancreatitis.

A critical obstacle to understanding the role of chronic pancreatitis in the development of pancreatic carcinoma is the lack of appropriate animal models for chronic pancreatitis which demonstrate similar clinical courses as in human patients. Cerulein (a cholecystokinin analog) can cause supramaximal stimulation of secretion and thus cause acute pancreatitis in the mouse [21]. Repetitive acute injury to the pancreas by cerulein in the mouse can reproduce some of the morphological characteristics of human chronic panreatitis such as acinar cell atrophy and fibrosis [29]. However, analysis of carcinogenesis-related molecules has not yet been done. Several transgenic models for pancreatitis have been also described [1, 9, 11, 28]. Two of them are based on genetic alterations found in human hereditary pancreatitis including the cationic trypsinogen gene and the cystic fibrosis transmembrane regulator gene [1, 11], but these models are limited by low penetrance (40% at 1 year of age) and significant latency of the phenotype. Marrache *et al.* [28] reported that the pancreas was atrophic and occasionally showed dilation of the pancreatic and biliary ducts secondary to proximal fibrotic stenosis in ElasshIL-1β (elastase promoter-driven human interleukin-1β) transgenic mice. However, forced expression of IL-1β does not reflect the situation in human patients.

Chronic pancreatitis is characterized by parenchymal changes including inflammation, fibrosis and loss of exocrine and endocrine tissue. Furthermore, acinar cells are replaced by metaplastic ductal lesions, called tubular complexes (TCs), which form complex arrangements with a monolayer of flattened duct-like cells [17, 22, 39]. Clinically, pain, maldigestion and diabetes mellitus occur as the result of long-standing pancreatic injury. Choline deficient ethionine-supplemented (CDE) diet is also known to induce acute hemorrhagic pancreatitis in mice [7, 14, 16, 30]. CDE diet-induced pancreatitis is considered to be an ideal model because of a similar natural history to that of the human disease as well as the histological and biochemical similarities [2]. However, there are no reports on CDE diet-induced chronic pancreatitis. In the cerulein model, cerulein should be injected every hour for six hours, followed by repeated injections twice every week for 10 weeks [29]. In contrast, feeding with CDE diet is easy.

In this manuscript, we used long-term administration of a CDE diet to develop a model of chronic pancreatitis and examined whether increased expression of carcinogenesis-related molecules was observed during chronic pancreatitis. This CDE diet model reproduced three key responses of human chronic pancreatitis: development of acinar atrophy, fibrosis and TCs which indicated that acinar cells acquired ductal cell characteristics. We also showed increased expression of carcinogenesis-related molecules.

Materials and Methods

Mice

Female C57BL/6J mice (starting at 8 weeks old) were housed in a climate-controlled room on a 12-h light-dark cycle (CLEA Japan, Inc., Tokyo, Japan). All procedures were approved by the Animal Care and Use Committee of Kumamoto University.

CDE diet-induced pancreatitis

Acute pancreatitis was induced by a CDE diet which was purchased from MP Biomedicals (catalog number; 960214, Solon, OH, USA), including vitamin free casein (10%), alpha soy protein (10%), DL-ethionine (0.5%), sucrose (56%), lard (20%) and mineral mix (3.5%).

Chronic lesions were induced by repeated acute pancreatitis episodes. Mice were fasted for 24 h (day 0) and then fed a CDE diet for 72 h (days 1 to 4; necrosis phase). Then, they were fed regular laboratory chow for 72 h (days 4 to 7; regeneration phase). We defined these 7 days as one cycle and tried to induce chronic pancreatitis by repeating the cycle (Fig.1A). Mice were sacrificed on days 0, 1, 4, 5 and 7 and pancreatea were rapidly extracted and prepared for the following studies on weeks 0, 4, 12, 16, 24, 32, and 54 after administration of the CDE diet (CDE diet group, n=3 per each period). As a control, we prepared age matched C57BL/6J mice fed regular laboratory chow (control diet group).

Histological analysis

Pancreatic tissues were fixed by 4% paraformaldehyde for 48 h, embedded in paraffin, sectioned, and stained with hematoxylin and eosin (HE) and azan staining. TCs were counted in ×100 high-power field per cut, 5 cuts per mouse. The area of the pancreas occupied by acinar cells was measured in whole pancreas on HE slides using ImageJ software (http://rsbweb.nih.gov/ij/).

Serum amylase activity

Mouse blood samples were collected on days 0, 1, 4, 5, and 7. Serum amylase levels were measured by SRL Inc., Tokyo, Japan. Substrate for measurement of pancreatic amylase activity was 2-chloro-4-nitrophenyl-4-galactopyranosylmaltoside (Gal-G2-CNP) (CicaLiquid-N p-AMY, Kanto Chemical Co., Inc., Tokyo, Japan).

Western blot analysis

Pancreas samples were homogenized in lysate buffer (50 mM Tris-HCl, pH 7.4, 150 mM NaCl, 1% Nonidet P-40, a protease inhibitor cocktail (1:100 dilution; Sigma-Aldrich, Tokyo, Japan) and a phosphatase inhibitor cocktail (1:100 dilution; Nacalai Tesque, Inc., Kyoto, Japan). Extracts (15 μg of protein per lane) underwent polyacrylamide gel electrophoresis and were transferred to Immobilon polyvinylidene difluoride membranes (Millipore, Billerica, MA, USA). After 1 h of incubation at room temperature in blocking buffer (TBS, 5% non-fat dry milk, 0.1% Tween-20), the membranes were incubated overnight at 4°C with primary antibodies to the antigens diluted in wash buffer (TBS, 0.1% Tween-20) containing 5% non-fat dry milk. Primary antibodies used were as follows: rabbit anti-mouse EGFR antibody (Cell Signaling Technology, Inc., Beverly, MA, USA), 1:1,000; rabbit anti-mouse phosphorylated-EGFR antibody (Cell Signaling Technology), 1:500; rabbit anti-mouse actin antibody (Sigma-Aldrich Corp., St. Louis, MO, USA), 1:1,000; rabbit anti-mouse serine protease inhibitor Kazal type 3 (Spink3) antibody [31], 1:1,000; goat anti-mouse amylase antibody (Santa Cruz Biotechnology, Inc., Santa Cruz, CA, USA), 1:2,000; rabbit anti-mouse trypsinogen antibody (Nordic Immunological Laboratories, Tilburg, Netherlands), 1:1,000; rabbit anti-mouse cyclooxygenase (Cox) 2 antibody (Cayman Chemical, Ann Arbor, MI, USA), 1:1,000; goat anti-mouse EGF antibody (R&D systems, Inc., Minneapolis, MN, USA), 1:1,000; and mouse anti-mouse TGF α antibody, 1:1,000 (Thermo Fisher Scientific, Fremont, CA, USA). In addition, the EZ-Detect Ras activation kit (Pierce Biotechnology, Rockford, IL, USA) was used to measure Ras activation. Membranes were then washed three times and incubated with secondary antibody [anti-rabbit immunoglobulin G antibody, 1:2,500 dilution (Amersham Biosciences Corp., Piscataway, NJ, USA) or anti-goat immunoglobulin G antibody, 1:5,000 dilution (Chemicon International, Inc., Billerica, MA, USA)] diluted in the antibody buffer for 1 h at room temperature, followed by three washes. Blots were developed with ECL Plus reagents (GE Healthcare, Buckinghamshire, UK). The band intensities were quantified by densitometry using ImageJ software, then normalized by the actin signals (n=3).

Statistical analysis

All data are expressed as mean ± standard error (SE). Statistical significance was determined by analysis of variance (ANOVA), followed by Dunnett's test. The differences were considered to be statistically significant at $P<0.05$.

Results

Histological changes of the pancreas in the acute phase after CDE diet

To analyze the initial reaction of the pancreas to the CDE diet, we examined histological changes during the one course of CDE diet treatment. As shown in Fig. 1B, evidence of acute pancreatitis, namely acinar cell necrosis with inflammatory infiltrates and interstitial edema, was induced after 72 h of CDE diet treatment. However, these pathological changes were restored to almost the normal state after the re-introduction of a normal diet (Fig. 1B). We also analyzed the serum amylase levels. The mean serum amylase level was 667 ± 33 U/l on Day 0, 1,067 ± 317 U/l on Day 1, 2,067 ± 252 U/l on Day 4 and 683 ± 83 U/l on Day 7. On day 4, a significant elevation in the serum amylase levels was observed compared with level on Day 0 ($P<0.05$) and returned to the basal level on Day 7. These results suggest that destruction and regeneration of pancreas occurred in one week.

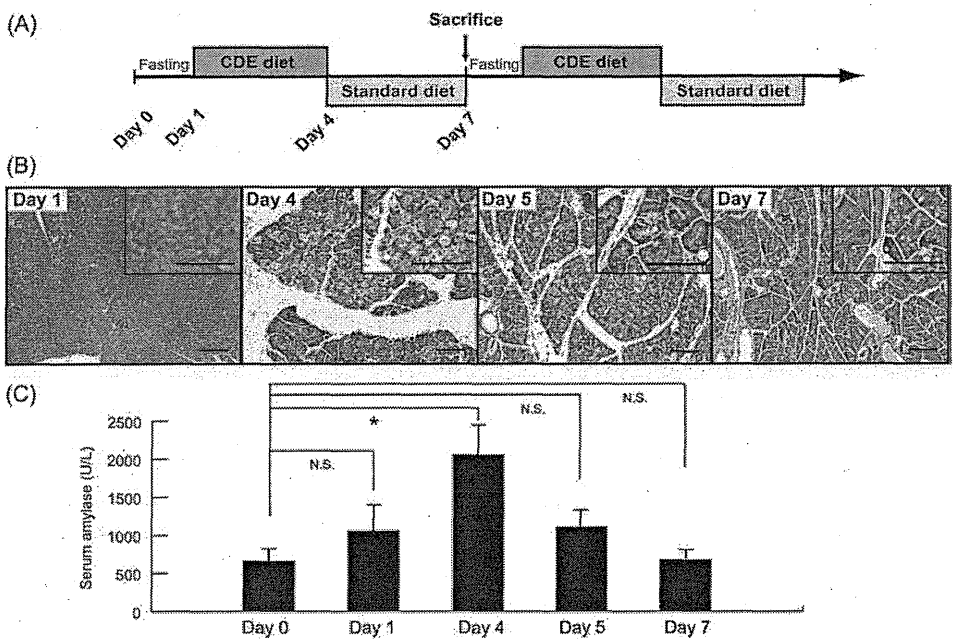

Fig. 1. Experimental protocol and histological changes of the pancreas in acute phase after one course of CDE diet treatment. A. Protocol for CDE diet. Mice were fasted for 24 h (Day 0) and then fed with a CDE diet for 72 h (Days 1 to 4; necrosis phase). Then, they were fed with regular laboratory chow for 72 h (Days 4 to 7; regeneration phase). B. Histological changes on Days 1, 4, 5, and 7. Scale bars: 100 μm. C. Serum amylase levels on Days 1, 4, 5, and 7 (n=3). Data represent mean ± SE. $^*P<0.05$.

Histological changes of the pancreas in the chronic phase after long-term CDE diet

We carefully analyzed the formation of TCs as well as acinar cell atrophy and fibrosis. Four (Fig. 2B) and twelve weeks (not shown) after starting the CDE diet, the histology was almost normal. After 16 weeks (Fig. 2C), TCs were formed in some areas. After 24 weeks, formation of TCs were remarkable (Fig. 2D and 2E). At this stage, chronic pancreatitis-like features characterized by well-developed TCs, acinar atrophy and fibrosis were established. On the 54th week, pancreatic glandular atrophy was observed (Fig. 2F and 2G). In addition, pancreatic acinar cells decreased in number and were replaced with interstitial tissues. In spite of the severe pancreatic degeneration, neoplastic changes were not observed. To evaluate pancreatic fibrosis, we performed azan staining. Although fibrous tissue around the TC was stained, the extent of the fibrosis was mild (Fig. 2H and 2I).

The number of TCs was 6.0 ± 1.4 at 12 weeks, 11.6 ± 1.7 at 16 weeks, 25.2 ± 4.2 at 24 weeks, 26.4 ± 2.0 at 32 weeks and 33.6 ± 5.6 at 54 weeks after starting the CDE diet; TCs were not observed in the control diet group (Fig. 3A). One-way ANOVA, indicated statistically significant increases in the number of TCs at 24, 32, and 54 weeks compared with the number at 4 weeks. In addition, we quantified the extent of acinar cell loss by morphometric analysis. In the control diet group, there was no significant decrease in acinar cell volume, although there was a slight decrease because of the increase in islet volume. In CDE-fed mice, the volume of acinar cells decreased gradually from 47 ± 6% at 24 weeks to 44 ± 16% at 32 weeks and 23 ± 5% after 54 weeks of CDE diet (Fig. 3B).

Activation of carcinogenesis-related molecules after long term CDE diet

We investigated the molecular events caused by long-term CDE diet using western blotting. EGFR overexpression, EGFR phosphorylation and *K-Ras* gene muta-

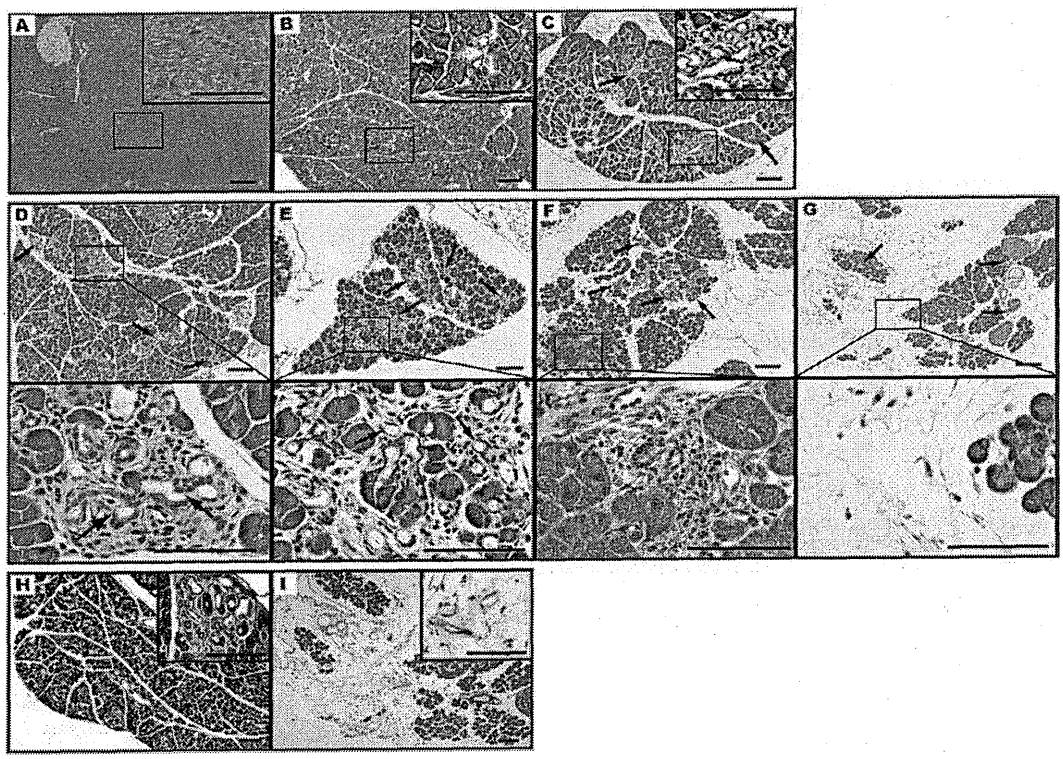

Fig. 2. Histological changes of the pancreas after long term CDE diet treatment. Mice were given regular laboratory chow (A) or CDE diet for 4 (B), 16 (C), 24 (D, E), or 54 (F, G) weeks. Pancreatic sections were analyzed by HE staining. Higher magnifications of the boxed areas at 24 and 54 weeks are shown in the lower column. Azan staining of pancreata from CDE diet mice is shown in H (24 weeks) and I (54 weeks). Arrows indicate tubular complexes. Scale bars: 100 μm.

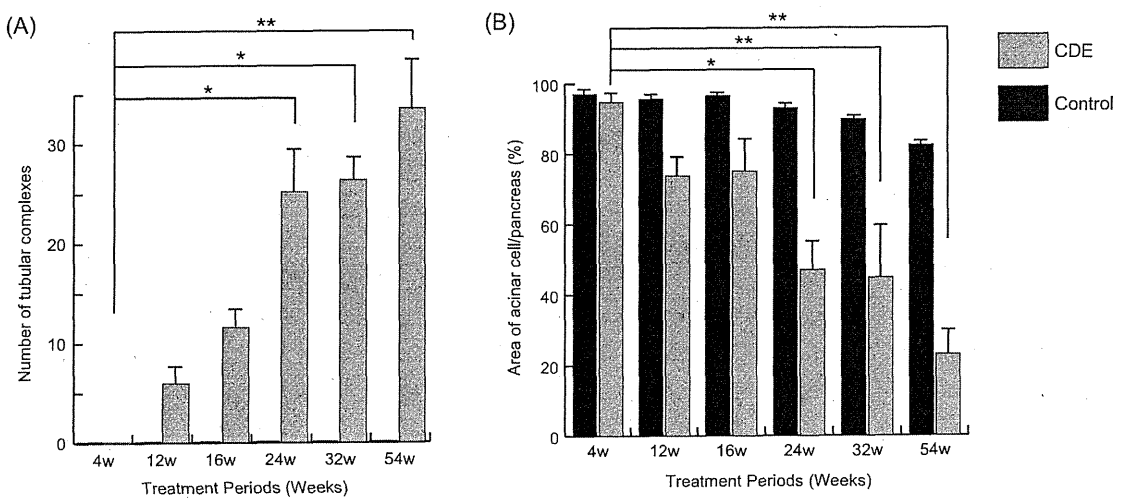

Fig. 3. Analysis of the number of tubular complexes and the volume of acinar cells. Number of tubular complexes (A) and volume of acinar cells (B) are shown for each treatment period. The black bar shows the control diet group, and the gray bar shows the CDE diet group. Data represent mean ± SE. (n=3, 5 cuts per mouse, $^{**}P<0.01$, $^{*}P<0.05$).

tions (activation of K-Ras molecule) are reported to be the key events in the process of pancreatic carcinogenesis. In the control diet group, there were no significant changes during the examination period (Fig. 4A). Compared with the control diet group, CDE diet induced overexpression and phosphorylation of EGFR after 4 weeks (Fig. 4B). The level of EGFR expression reached its peak at 12 to 16 weeks and declined after 32 weeks. Activation of the K-Ras molecule was also detected after 12 weeks. Expression patterns of EGF, TGF α, and Spink3, one of the potent ligands for EGFR [34], were similar to that of EGFR. The expression of EGF followed a similar course, but was weaker than that of the other ligands for EGFR. We also investigated the expression of Cox 2 as a parameter of inflammatory responses. Cox 2 was also overexpressed in a manner similar to EGFR in the mice fed the long-term CDE diet. There were no significant changes in amylase and trypsinogen levels related to the CDE diet (Fig. 4).

Discussion

In this study, we developed a model of chronic pancreatitis that reproduces three key responses of human chronic pancreatitis: development of acinar atrophy, fibrosis, and TCs. We also demonstrated the expression of EGFR and its potent ligands, phosphorylation of EGFR, and the activation of K-Ras in the step of chronic inflammation.

Compared with other experimental models, CDE diet-induced pancreatitis is considered to be an ideal model because of its similar natural history to that of the human disease as well as histological and biochemical similarities [2]. The mechanism of acute pancreatitis development in the mice fed the CDE diet remains unclear. It is likely that ethionine disrupts phospholipid metabolism of membranes that are involved in the processes of intracellular transport and secretion of pancreatic enzymes. A choline-deficient diet would potentiate the activity of ethionine in this respect, because a choline-deficient diet also induces changes in membrane phospholipids of cellular organelles [8, 23, 24]. Thus, normal luminal exocytosis appeared to be blocked, and subsequently zymogen granules accumulated in the cytoplasm [14, 18]. These changes may result in activation of zymogens eventually leading to pancreatitis. In any case, the CDE-diet model is simple and easy to prepare, and thus seems to be a promising model for studies of chronic pancreatitis.

As far as we know, this is the first report on the expression of carcinogenesis-related molecules such as EGFR, K-Ras, Cox 2, and TGF α, during chronic pancreatitis. Their expression started to increase at 4 weeks and reached their peaks at 12 and 16 weeks in the CDE diet model. Expression of these molecules decreased after 32 weeks. This may have been due to the decrease in the number of normally functioning pancreatic cells as demonstrated in Fig. 3B. EGFR and its ligand, TGF α, as well as PDA, are frequently overexpressed in human pancreatic tissues obtained from patients with chronic pancreatitis [20, 34]. The rate of *K-Ras* gene mutation increases along with disease progression in chronic pancreatitis, and the mutations are found in nearly 100% of PDA [3]. Furthermore, EGFR induction occurs in low-grade pancreatic intra-epithelial neoplasias, indicating that autocrine EGF-family growth signaling is operative at the earliest stage of pancreatic neoplasia [3]. Nevertheless, PDA did not develop in our model, even after 54 weeks. On the other hand, TCs were formed with advancing age. TCs are considered to be precursor lesions of PDA [15, 35], and they have often been observed in human/rodent chronic pancreatitis and PDA [5, 6, 12, 15, 36, 37]. There is one report in which the transition from chronic inflammation to metaplasia/dysplasia is described [9]. Colby *et al.* [9] reported that Cox 2 overexpression driven by the bovine keratin 5 promoter led to acinar-to-ductal metaplasia, increased proliferation of metaplastic ductal cells, and nuclear pleomorphisms accompanied the elevation of prostaglandin E_2 (PGE_2). Because PGE_2 confers both survival and growth advantages, it may act as an inhibitor of apoptosis or a promoter of proliferation. We demonstrated the overexpression of Spink3 along with EGFR in western blot analysis. We previously demonstrated that the human serine protease inhibitor, Kazal type 1 (SPINK1: mouse homolog Spink3) can bind to EGFR and work as a growth factor through EGFR [34]. Thus, Spink3 may act as a growth factor, leading to cell proliferation and regeneration of tissue structure. In any case, chronic pancreatitis itself is not sufficient for the development

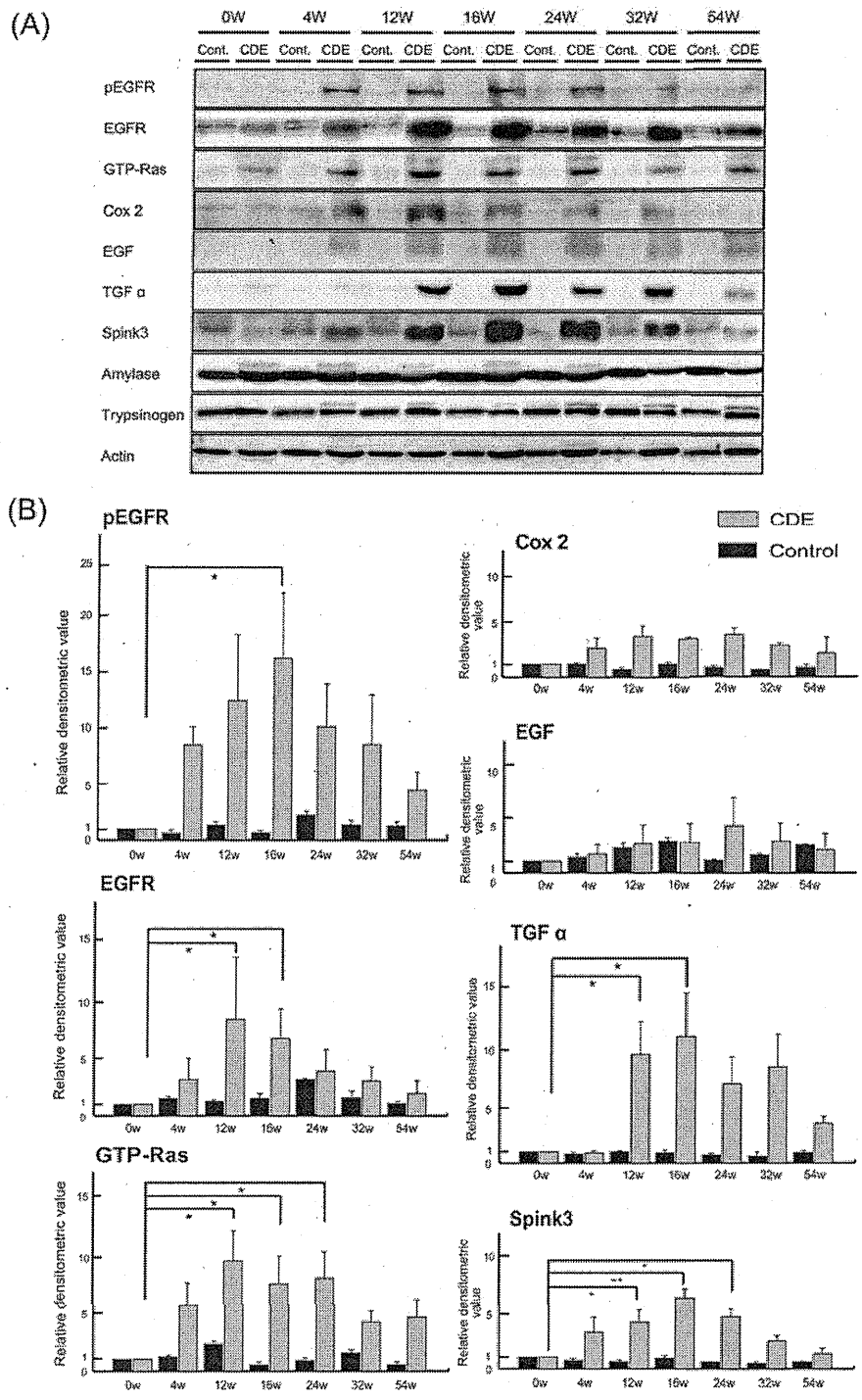

Fig. 4. Expression pattern of inflammation and/or carcinogenesis-related molecules. A. Western blot analysis was performed using the antibodies as described in Materials and Methods. B. Densitometric analysis for pEGFR, EGFR, GTP-Ras, Cox 2, TGF α, and Spink3 before and after CDE diet by western blot. Data are expressed as the magnification of activity in the control before CDE diet after normalization by the actin signals. Only the data with significant differences are shown. Cont.: control diet group. CDE: CDE diet group. EGFR; epidermal growth factor receptor, pEGFR; phosphorylated EGFR, GTP-Ras; activated K-Ras, Cox 2; cyclooxygenase 2, EGF; epidermal growth factor, TGF α; transforming growth factor α, Spink3; serine protease inhibitor, Kazal type 3 (n=3, $^{**}P<0.01$, $^{*}P<0.05$).

of PDA. Further combinations of CDE diet with the administration of other promotion insults or genetic alterations may result in PDA development.

Acknowledgments

We wish to thank Ms. Yumi Ohtake for her technical assistance. This work was supported by a Grant-in-Aid for Scientific Research Priority Areas (KAKENHI) (17012018) and a Grant-in Aid for Scientific Research (S) (21220010) from Japan Society for the Promotion of Science (JSPS).

References

1. Archer, H., Jura, N., Keller, J., Jacobson, M., and Bar-Sagi, D. 2006. A mouse model of hereditary pancreatitis generated by transgenic expression of R122H trypsinogen. *Gastroenterology* 131: 1844–1855.
2. Banerjee, A.K., Galloway, S.W., and Kingsnorth, A.N. 1994. Experimental models of acute pancreatitis. *Br. J. Surg.* 81: 1096–1103.
3. Bardeesy, N. and DePinho, R.A. 2002. Pancreatic cancer biology and genetics. *Nat. Rev. Cancer* 2: 897–909.
4. Barton, C.M., Hall, P.A., Hughes, C.M., Gullick, W.J., and Lemoine, N.R. 1991. Transforming growth factor alpha and epidermal growth factor in human pancreatic cancer. *J. Pathol.* 163: 111–116.
5. Bockman, D.E., Boydston, W.R., and Anderson, M.C. 1982. Origin of tubular complexes in human chronic pancreatitis. *Am. J. Surg.* 144: 243–249.
6. Bockman, D.E., Guo, J., Buchler, P., Muller, M.W., Bergmann, F., and Friess, H. 2003. Origin and development of the precursor lesions in experimental pancreatic cancer in rats. *Lab. Invest.* 83: 853–859.
7. Callicutt, C.S., Sabek, O., Fukatsu, K., Lundberg, A.H., Gaber, L., Wilcox, H., Kotb, M., and Gaber, A.O. 2003. Diminished lung injury with vascular adhesion molecule-1 blockade in choline-deficient ethionine diet-induced pancreatitis. *Surgery* 133: 186–196.
8. Chen, S.H., Estes, L.W., and Lombardi, B. 1972. Lecithin depletion in hepatic microsomal membranes of rats fed on a choline-deficient diet. *Exp. Mol. Pathol.* 17: 176–186.
9. Colby, J.K., Klein, R.D., McArthur, M.J., Conti, C.J., Kiguchi, K., Kawamoto, T., Riggs, P.K., Pavone, A.I., Sawicki, J., and Fischer, S.M. 2008. Progressive metaplastic and dysplastic changes in mouse pancreas induced by cyclooxygenase-2 overexpression. *Neoplasia* 10: 782–796.
10. Day, J.D., Digiuseppe, J.A., Yeo, C., Lai-Goldman, M., Anderson, S.M., Goodman, S.N., Kern, S.E., and Hruban, R.H. 1996. Immunohistochemical evaluation of HER-2/neu expression in pancreatic adenocarcinoma and pancreatic intraepithelial neoplasms. *Hum. Pathol.* 27: 119–124.
11. Durie, P.R., Kent, G., Phillips, M.J., and Ackerley, C.A. 2004. Characteristic multiorgan pathology of cystic fibrosis in a long-living cystic fibrosis transmembrane regulator knockout murine model. *Am. J. Pathol.* 164: 1481–1493.
12. Esposito, I., Seiler, C., Bergmann, F., Kleeff, J., Friess, H., and Schirmacher, P. 2007. Hypothetical progression model of pancreatic cancer with origin in the centroacinar-acinar compartment. *Pancreas* 35: 212–217.
13. Friess, H., Berberat, P., Schilling, M., Kunz, J., Korc, M., and Buchler, M.W. 1996. Pancreatic cancer: the potential clinical relevance of alterations in growth factors and their receptors. *J. Mol. Med.* 74: 35–42.
14. Gilliland, L. and Steer, M.L. 1980. Effects of ethionine on digestive enzyme synthesis and discharge by mouse pancreas. *Am. J. Physiol.* 239: G418–426.
15. Jimenez, R.E., Z'Graggen, K., Hartwig, W., Graeme-Cook, F., Warshaw, A.L., and Fernandez-del Castillo, C. 1999. Immunohistochemical characterization of pancreatic tumors induced by dimethylbenzanthracene in rats. *Am. J. Pathol.* 154: 1223–1229.
16. Kihara, Y., Yoshikawa, H., Honda, H., Fukumitsu, K., Yamaguchi, T., and Otsuki, M. 2005. Natural disruption of group 2 phospholipase A2 gene protects against choline-deficient ethionine-supplemented diet-induced acute pancreatitis and lung injury. *Pancreas* 31: 48–53.
17. Kloppel, G. and Maillet, B. 1993. Pathology of acute and chronic pancreatitis. *Pancreas* 8: 659–670.
18. Koike, H., Steer, M.L., and Meldolesi, J. 1982. Pancreatic effects of ethionine: blockade of exocytosis and appearance of crinophagy and autophagy precede cellular necrosis. *Am. J. Physiol.* 242: G297–307.
19. Korc, M., Chandrasekar, B., Yamanaka, Y., Friess, H., Buchler, M., and Beger, H.G. 1992. Overexpression of the epidermal growth factor receptor in human pancreatic cancer is associated with concomitant increases in the levels of epidermal growth factor and transforming growth factor alpha. *J. Clin. Invest.* 90: 1352–1360.
20. Korc, M., Friess, H., Yamanaka, Y., Kobrin, M.S., Buchler, M., and Beger, H.G. 1994. Chronic pancreatitis is associated with increased concentrations of epidermal growth factor receptor, transforming growth factor alpha, and phospholipase C gamma. *Gut* 35: 1468–1473.
21. Lampel, M. and Kern, H.F. 1977. Acute interstitial pancreatitis in the rat induced by excessive doses of a pancreatic secretagogue. *Virchows Arch. A Pathol. Anat. Histol.* 373: 97–117.
22. Lechene de la Porte, P., Iovanna, J., Odaira, C., Choux, R., Sarles, H., and Berger, Z. 1991. Involvement of tubular complexes in pancreatic regeneration after acute necrohemorrhagic pancreatitis. *Pancreas* 6: 298–306.
23. Leelavathi, D.E., Katyal, S.L., and Lombardi, B. 1974. Lecithin depletion in liver mitochondria of rats fed a choline-deficient diet. Effect on beta-hydroxybutyrate dehydrogenase. *Life Sci.* 14: 1203–1210.
24. Lombardi, B. 1971. Effects of choline deficiency on rat hepatocytes. *Fed. Proc.* 30: 139–142.
25. Lowenfels, A.B., Maisonneuve, P., Cavallini, G., Ammann, R.W., Lankisch, P.G., Andersen, J.R., Dimagno, E.P.,

Andren-Sandberg, A., and Domellof, L. 1993. Pancreatitis and the risk of pancreatic cancer. International Pancreatitis Study Group. *N. Engl. J. Med.* 328: 1433–1437.

26. Lowenfels, A.B., Maisonneuve, P., DiMagno, E.P., Elitsur, Y., Gates, L.K. Jr., Perrault, J., and Whitcomb, D.C. 1997. Hereditary pancreatitis and the risk of pancreatic cancer. International Hereditary Pancreatitis Study Group. *J. Natl. Cancer Inst.* 89: 442–446.
27. Malka, D., Hammel, P., Maire, F., Rufat, P., Madeira, I., Pessione, F., Levy, P., and Ruszniewski, P. 2002. Risk of pancreatic adenocarcinoma in chronic pancreatitis. *Gut* 51: 849–852.
28. Marrache, F., Tu, S.P., Bhagat, G., Pendyala, S., Osterreicher, C.H., Gordon, S., Ramanathan, V., Penz-Osterreicher, M., Betz, K.S., Song, Z., and Wang, T.C. 2008. Overexpression of interleukin-1beta in the murine pancreas results in chronic pancreatitis. *Gastroenterology* 135: 1277–1287.
29. Neuschwander-Tetri, B.A., Burton, F.R., Presti, M.E., Britton, R.S., Janney, C.G., Garvin, P.R., Brunt, E.M., Galvin, N.J., and Poulos, J.E. 2000. Repetitive self-limited acute pancreatitis induces pancreatic fibrogenesis in the mouse. *Dig. Dis. Sci.* 45: 665–674.
30. Niederau, C., Luthen, R., Niederau, M.C., Grendell, J.H., and Ferrell, L.D. 1992. Acute experimental hemorrhagic-necrotizing pancreatitis induced by feeding a choline-deficient, ethionine-supplemented diet. Methodology and standards. *Eur. Surg. Res.* 24: 40–54.
31. Ohmuraya, M., Hirota, M., Araki, M., Mizushima, N., Matsui, M., Mizumoto, T., Haruna, K., Kume, S., Takeya, M., Ogawa, M., Araki, K., and Yamamura, K. 2005. Autophagic cell death of pancreatic acinar cells in serine protease inhibitor Kazal type 3-deficient mice. *Gastroenterology* 129: 696–705.
32. Oikawa, T., Hitomi, J., Kono, A., Kaneko, E., and Yamaguchi, K. 1995. Frequent expression of genes for receptor tyrosine kinases and their ligands in human pancreatic cancer cells. *Int. J. Pancreatol.* 18: 15–23.
33. Overholser, J.P., Prewett, M.C., Hooper, A.T., Waksal, H.W., and Hicklin, D.J. 2000. Epidermal growth factor receptor blockade by antibody IMC-C225 inhibits growth of a human pancreatic carcinoma xenograft in nude mice. *Cancer* 89: 74–82.
34. Ozaki, N., Ohmuraya, M., Hirota, M., Ida, S., Wang, J., Takamori, H., Higashiyama, S., Baba, H., and Yamamura, K. 2009. Serine protease inhibitor, Kazal type 1, promotes proliferation of pancreatic cancer cells through the epidermal growth factor receptor. *Mol. Cancer Res.* (in press).
35. Parsa, I., Longnecker, D.S., Scarpelli, D.G., Pour, P., Reddy, J.K., and Lefkowitz, M. 1985. Ductal metaplasia of human exocrine pancreas and its association with carcinoma. *Cancer Res.* 45: 1285–1290.
36. Strobel, O., Dor, Y., Alsina, J., Stirman, A., Lauwers, G., Trainor, A., Castillo, C.F., Warshaw, A.L., and Thayer, S.P. 2007. In vivo lineage tracing defines the role of acinar-to-ductal transdifferentiation in inflammatory ductal metaplasia. *Gastroenterology* 133: 1999–2009.
37. Wagner, M., Luhrs, H., Kloppel, G., Adler, G., and Schmid, R.M. 1998. Malignant transformation of duct-like cells originating from acini in transforming growth factor transgenic mice. *Gastroenterology* 115: 1254–1262.
38. Watanabe, M., Nobuta, A., Tanaka, J., and Asaka, M. 1996. An effect of K-ras gene mutation on epidermal growth factor receptor signal transduction in PANC-1 pancreatic carcinoma cells. *Int. J. Cancer* 67: 264–268.
39. Willemer, S. and Adler, G. 1989. Histochemical and ultrastructural characteristics of tubular complexes in human acute pancreatitis. *Dig. Dis. Sci.* 34: 46–55.

J Gastroenterol (2010) 45:1241–1246
DOI 10.1007/s00535-010-0285-6

ORIGINAL ARTICLE—LIVER, PANCREAS, AND BILIARY TRACT

Detection of liver metastases secondary to pancreatic cancer: utility of combined helical computed tomography during arterial portography with biphasic computed tomography-assisted hepatic arteriography

Yoshiaki Ikuta · Hiroshi Takamori · Osamu Ikeda · Hiroshi Tanaka · Yasuo Sakamoto · Daisuke Hashimoto · Nobuyuki Ozaki · Osamu Nakahara · Satoshi Furuhashi · Shinya Abe · Toru Beppu · Shinya Shimada · Yasuyuki Yamashita · Hideo Baba

Received: 3 December 2009 / Accepted: 28 May 2010 / Published online: 16 July 2010

Abstract
Background This study was designed to define the diagnostic advantage of computed tomography during arterial portography (CTAP) combined with computed tomography–assisted hepatic arteriography (CTHA) for the preoperative detection of liver metastases secondary to pancreatic cancer compared with that of multidetector computed tomography (MDCT).
Methods From January 2002 to December 2007, we retrospectively studied 197 consecutive patients with pancreatic cancer. MDCT was performed on 192 patients prior to preoperative visceral angiography; 153 patients underwent CTAP + CTHA at the time of preoperative angiography.
Results Liver metastases were identified in 39 patients by means of MDCT. Of the 153 patients who had no evidence of liver metastases on MDCT, 129 patients underwent CTAP + CTHA, and 53 of these 129 patients (41.1%) were diagnosed as having liver metastases that could not be detected by MDCT. These tumors missed by MDCT ranged from 3 to 15 mm in size. On CTAP + CTHA, a solitary nodule in the liver was detected in 11 patients, 2 nodules were detected in 6 patients, 3 lesions were detected in 2 patients, and ≧4 lesions were detected in 34 patients. The sensitivity and specificity of CTAP + CTHA versus MDCT were 94.2 versus 48.4% and 82.7 versus 97.9%, respectively.
Conclusions The combination of CTAP and CTHA is useful to confirm liver metastases and can potentially offer more accurate staging of pancreatic cancer compared with MDCT.

Keywords Pancreatic cancer · Liver metastasis · CTHA · CTAP

Y. Ikuta · H. Takamori · H. Tanaka · Y. Sakamoto · D. Hashimoto · N. Ozaki · O. Nakahara · S. Furuhashi · S. Abe · T. Beppu · H. Baba (✉)
Department of Gastroenterological Surgery, Graduate School of Medical Sciences, Kumamoto University, 1-1-1 Honjo, Kumamoto 860-8556, Japan
e-mail: hdobaba@kumamoto-u.ac.jp

O. Ikeda · Y. Yamashita
Department of Diagnostic Radiology, Graduate School of Medical Sciences, Kumamoto University, Kumamoto, Japan

S. Shimada
Department of Surgery, Yatsushiro Social Insurance General Hospital, Kumamoto, Japan

Introduction

The prognosis of pancreatic adenocarcinoma still remains dismal, with a 5-year survival rate of 4% [1]. Despite improvements in imaging technology, fewer than 20% of all patients will be potentially resectable at the time of the initial diagnosis [1, 2]. Complete pancreatic resection can yield actuarial 5-year survival rates of 15–25% following pancreaticoduodenectomy [3–5] and 8–14% following distal pancreatectomy [6, 7]. Although surgery is the only curative treatment, even after curative resection of pancreatic carcinoma, most patients have a recurrence, including approximately 62% with liver metastases [8, 9]. The high recurrence rate of liver metastases in the early period after surgery suggests that liver metastases may have been present at the time of operation but below the threshold (microscopic) of detection by current preoperative radiological imaging and intraoperative examination. Therefore, more precise evaluation for hepatic lesions is necessary, because accurate detection of liver metastases

has major implications in guiding both appropriate treatment and defining prognosis.

We have previously reported the effectiveness of computed tomography during arterial portography combined with computed tomography-assisted hepatic arteriography (CTAP + CTHA) in detecting liver metastases from pancreatic cancer [10]. The present study, which included a large number of pancreatic cancer patients, was designed to evaluate the diagnostic advantage of CTAP + CTHA for the preoperative detection of liver metastases compared with that of multidetector computed tomography (MDCT).

Methods

We retrospectively studied 197 consecutive patients with pancreatic cancer from January 2002 to December 2007. Of the 197 patients, 192 underwent MDCT.

All CT scans were obtained with 4-slice MDCT (Lightspeed QXi; General Electric Medical Systems, Milwaukee, WI, USA). Imaging parameters were established as a pitch of 3 with a table speed of 15.0 mm/rotation to visualize the arterial phase and portal venous phase. All phases were acquired in a cranial-to-caudal direction. An 18- or 20-gauge intravenous catheter was placed in the patient's antecubital vein. A total of 100–120 mL iopamidol 300 (Iopamiron; Nihon Schering, Osaka, Japan) was infused using a power injector at a rate of 3 to 4 mL/s. Thirty seconds after the start of the infusion, entire liver imaging was performed during a breath-hold. Subsequently, the portal venous phase was obtained following a scan delay of 70 s. Each image was reconstructed with contiguous 5-mm slice thickness.

CTAP + CTHA was performed at the time of preoperative angiography after no remote metastasis was confirmed on CT. All studies were performed with an IVR-CT system (Toshiba Medical Systems, Tochigi, Japan), which comprised a digital subtraction angiography system (KXO-80C/DFP-2000A; Toshiba Medical Systems) and a helical CT scanner (X-Vision; Toshiba Medical Systems). This equipment is capable of performing digital subtraction angiography and CT scanning with the patient in one position. A 5-French catheter was inserted via the right femoral artery with the Seldinger technique, followed by positioning the tip of the catheter in the superior mesenteric artery, and testing the infusion capacity of the vessel. Subsequently, helical CT during the injection of the contrast medium into the superior mesenteric artery was performed for CTAP. CTAP was performed using 90 mL of contrast material (Optiray 160; Tyco Japan, Tokyo, Japan) injected at a rate of 2.5 mL/s. The CT scanning was performed 25 s after the start of the injection.

For CTHA, the tip of the catheter was placed in the common hepatic artery and biphasic CT was performed during the injection of the contrast medium into this artery, starting at 5 s after the start of the injection. CTHA was performed using 45 mL of Optiray 160 injected at a rate of 1.5 mL/s.

In all patients, MDCT and CTAP + CTHA studies were performed within 2 weeks.

All MDCT scans were reviewed by 2 experienced abdominal radiologists in consultation. At the MDCT reading, the readers knew that the patients had pancreatic carcinoma, but information about liver metastases was not given. They evaluated images of combinations of plain, arterial phase, and portal venous phase images of MDCT. CTAP + CTHA images were evaluated independently just after the examination by different experienced radiologists in consultation. Lesions that were hypoattenuated on CTAP and enhanced on CTHA were diagnosed as liver metastases. The presence of each lesion at diagnosis was defined as positive by histological proof, intraoperative ultrasonography (IOUS), bimanual palpation at operation, or enlargement of the lesions during the follow-up period on radiological examinations. The absence of liver metastasis at diagnosis was proved by intraoperative findings for operative cases and/or follow-up radiological examinations performed at intervals of more than 6 months.

Results

The characteristics of the 192 patients are outlined in Table 1. There were 76 women and 116 men in this study. The median age of the patients was 64.5 years (range 34–86). Of the 192 patients, 182 had extrapancreatic disease (29 with category T3, 153 with T4) according to the General

Table 1 Patients' characteristics

No. of patients	192
Age (years)	
Median	64.5
Range	34-86
Male/female	116/76
Extension of primary tumor[a]	
T1	5
T2	5
T3	29
T4	153
Site of primary lesion	
Head	118
Body	51
Tail	23

[a] According to the General Rules for the Study of Pancreatic Cancer of the Japan Pancreas Society classification

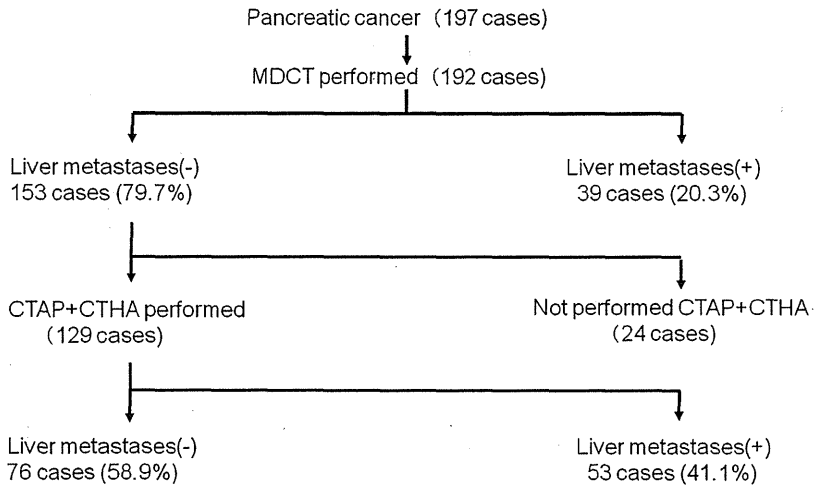

Fig. 1 Schematic diagram of the preoperative diagnoses of liver metastases secondary to pancreatic cancer by multidetector computed tomography (*MDCT*) and computed tomography during arterial portography (*CTAP*) + computed tomography–assisted hepatic arteriography (*CTHA*). Liver metastases were detected by MDCT in 39 patients (20.3%). Of the 153 patients who had no evidence of liver metastases on MDCT, 129 patients underwent CTAP + CTHA. Of the 129 patients who underwent CTAP + CTHA, liver metastases were detected in 53 patients (41.1%)

Rules for the Study of Pancreatic Cancer of the Japan Pancreas Society classification. The pancreatic tumor was limited to the pancreas in 10 patients (5 with T1, 5 with T2). The primary lesion of the pancreas was located in the head for 118 patients, in the body for 51, and in the tail for 23 patients (Table 1).

Figure 1 is a schematic diagram of the preoperative diagnoses of liver metastases secondary to pancreatic cancer with MDCT and CTAP + CTHA in this study. Liver metastases were detected by MDCT in 39 patients (20.3%). The size of these lesions ranged from 5 to 80 mm (mean 28 ± 20 mm). Of these 39 patients, 25 underwent CTAP + CTHA. CTAP + CTHA could also detect these liver metastases in all the patients. Of the 153 patients who had no evidence of liver metastases on MDCT, 129 patients underwent CTAP + CTHA. Of the remaining 24 patients, 9 underwent surgery without CTAP + CTHA being performed. Of these 9 patients, 2 suffered from liver metastases 2 and 4 months, respectively, after pancreatic resection, and liver metastasis was detected in one patient at surgery.

Of the 129 patients who underwent CTAP + CTHA, liver metastases were detected in 53 patients (41.1%). These liver metastases that were not detected by MDCT ranged from 3 to 15 mm (mean 6.2 ± 2.9 mm) in size (Fig. 2). Most of them were within 10 mm in diameter. On CTAP + CTHA, a solitary nodule in the liver was detected in 11 patients, 2 nodules were detected in 6 patients, 3 lesions were detected in 2 patients, and multiple lesions were detected in 34 patients. Four of the 53 patients underwent laparotomy, and hepatic nodules were confirmed at the same site as those detected by CTAP + CTHA. As shown in Fig. 3, in a 70-year-old woman with

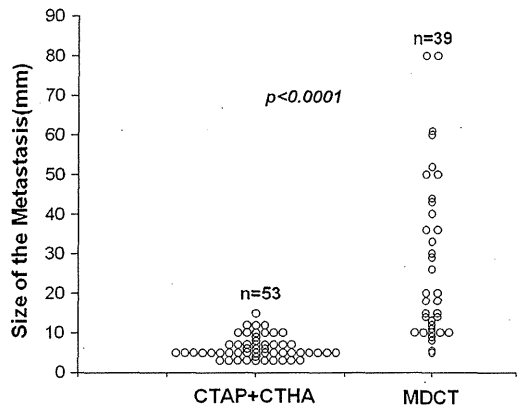

Fig. 2 Comparison of the sizes of the liver metastases. Liver metastases were detected by MDCT in 39 patients. The size of these lesions ranged from 5 to 80 mm (mean 28 ± 20 mm). In 53 patients whose metastases could not be detected by MDCT, liver metastases could be detected by CTAP + CTHA. The size of these lesions ranged from 3 to 15 mm (6.2 ± 2.9 mm). Most of them were within 10 mm in diameter

liver metastasis from cancer of the body of the pancreas, a 5-mm hypoattenuated lesion was detected in segment 3 of the liver by CTAP. This lesion was enhanced by CTHA but was not detected by MDCT. This patient underwent pancreatectomy, and the hepatic nodule was confirmed histologically as liver metastasis from pancreatic cancer.

We confirmed no liver metastases by intraoperative findings in 55 patients. For the remaining 137 patients, follow-up radiological examination revealed the absence of liver metastases.

Of the 76 patients in whom no liver metastases were detected by either MDCT or CTAP + CTHA, 42 underwent

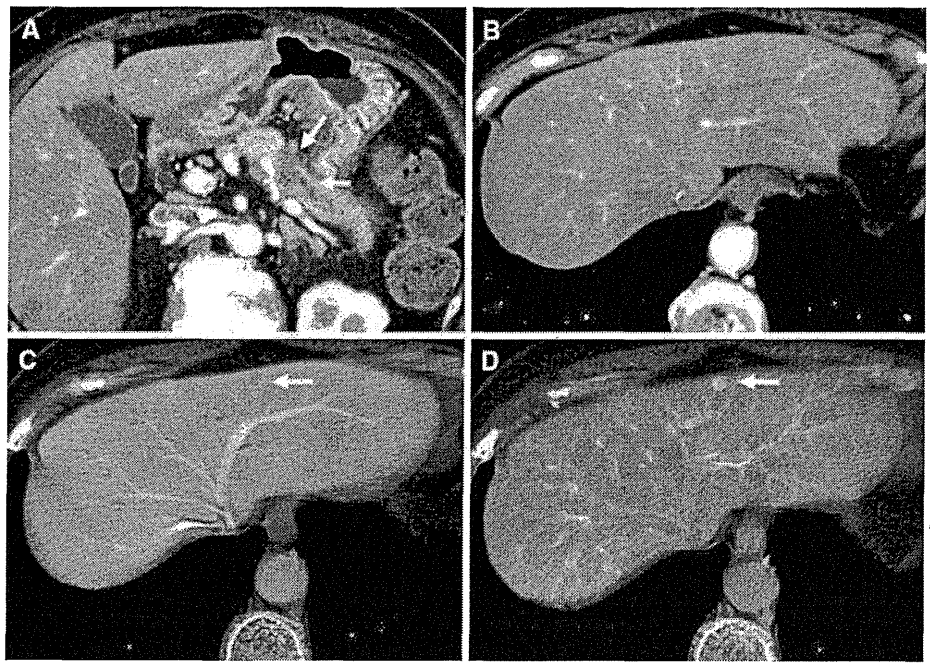

Fig. 3 Imaging in a 70-year-old woman with liver metastasis from cancer of the body of the pancreas. **a** MDCT shows a hypovascular mass in the body of the pancreas (*arrows*). **b** MDCT could not detect liver metastasis. **c** A 5-mm hypoattenuated lesion is noted on the CTAP scan in segment 3 (*arrow*). **d** CTHA shows a focally enhanced lesion, which is in the same place as the lesion detected by CTAP (*arrow*)

pancreatectomy. Only 2 of these 42 patients had liver metastases that were detected by MDCT within 6 months after pancreatectomy. Among the remaining 34 patients, only 1 patient had liver metastases that were detected by MDCT within 6 months after pancreatectomy; therefore, of these 76 patients, 73 (96.1%) were considered to be "true negative".

Table 2 summarizes comparisons of the diagnostic accuracy of liver metastasis detected by MDCT and CTAP + CTHA. Of the 192 patients, 35 were excluded from the analyses of diagnostic accuracy, because they died of advanced disease within 6 months of the pancreatectomy. Of these 35 patients 2 had undergone CTAP + CTHA. Of the 127 assessable patients for whom CTAP + CTHA had been performed, 111 (87.4%) were diagnosed accurately. Of the 65 patients who were diagnosed as having no liver metastases by CTAP + CTHA, 3 suffered from liver metastases, and metastases could not be detected more than 6 months after the surgery in the other 62 patients. On the other hand, of the 62 patients diagnosed as having liver metastases by CTAP + CTHA, metastases could not be detected within 6 months after the first CTAP + CTHA in 13 patients. The sensitivity and specificity of CTAP + CTHA versus MDCT were 94.2% (49 of 52) versus 48.4% (30 of 62) and 82.7% (62 of 75) versus 97.8% (93 of 95), respectively.

Table 2 Detection of liver metastases

	MDCT (n = 157)	CTAP + CTHA (n = 127)
Sensitivity	48.4% (30/62)	94.2% (49/52)
Specificity	97.9% (93/95)	82.7% (62/75)
Positive PV	93.8% (30/32)	75.0% (49/62)
Negative PV	74.4% (93/125)	95.4% (62/65)
Overall accuracy	78.3% (123/157)	87.4% (111/127)

MDCT multidetector computed tomography, *CTAP* computed tomography during arterial portography, *CTHA* computed tomography–assisted hepatic arteriography, *PV* predictive value

Discussion

We have already reported that more than 50% of patients were diagnosed as having liver metastases by CTAP + CTHA in whom these metastases were not detected by MDCT [10]. In that study, although the number of patients was small, we concluded that the combination of CTAP + CTHA improved the detection of liver metastases secondary to pancreatic cancer [10] . Therefore, in the present study, we analyzed a large number of patients with pancreatic cancer. The major finding of the present study was that the combination of CTAP and CTHA has sensitivity superior to that of MDCT for the preoperative diagnosis of liver metastases from pancreatic cancer.

CTAP + CTHA have been the most sensitive nonsurgical imaging techniques for the detection of hepatic metastases [11–14]. The sensitivity of CTAP + CTHA was 94.2% in the present study, which is comparable with those in other trials (72–95.8%) [15–18]. On the other hand, the sensitivity of MDCT, at 48.4%, was too low a level. Bhattacharjya et al. [15] reported that CTAP detected more lesions than MDCT but the difference was not statistically significant. However, they also reported that magnetic resonance imaging (MRI) and CTAP were

significantly better than MDCT in detecting multiple lesions. Satoi et al. [18] reported that MDCT was better for detecting liver metastases of pancreatic cancer than CTAP + CTHA. These conclusions appear to be based on MDCT findings derived from comparisons of 1.25-mm-thick vs 5-mm-thick contiguous slices. However, the sensitivity of CTAP + CTHA in the study of Satoi et al. [18] was considerably low (72.0%) compared with that in other trials, and their study contained only a small number of patients (25 cases).

The disadvantages of CTAP + CTHA are its low specificity, the need for technical experts in performing the imaging, the cost, and the relative invasiveness [16, 18]. CTAP and CTHA require a larger quantity of contrast medium than MDCT. However, in our study, no patients experienced renal dysfunction after CTAP + CTHA. Therefore, it seems that CTAP + CTHA could be performed in all patients, although we should monitor patients' renal function.

In our hospital, we have been using combination chemotherapy with intraarterial 5-fluorouracil infusion combined with systemic gemcitabine for patients with unresectable pancreatic cancer, and the combination is well tolerated and seems to be effective [19]. In the present study, the false-positive rate was 21% (13 out of 62). This is a relatively high rate. The specificity of CTAP + CTHA is relatively low, because on CTAP + CTHA some chronic liver damage or an intrahepatic arterioportal shunt may be depicted as the presence of liver metastases. Also, we thought that the false positivity occurred because all the 13 patients received chemotherapy after diagnosis. These patients received systemic administration of gemcitabine combined with continuous arterial infusion of 5-fluorouracil. Therefore, some metastases may have disappeared because the chemotherapy was effective during the follow-up period.

In the present study, 41.1% of liver metastases that could not be detected by MDCT were detected by CTAP + CTHA. The size of these metastatic lesions was within 15 mm, and most of these lesions were within 10 mm in diameter. Liver metastases secondary to pancreatic cancer have often been detected as multiple and small lesions, especially when they are within 10 mm in diameter. Bhattacharjya et al. [15] reported that CTAP could detect smaller metastases (<1 cm) than CT and MRI. Jimenez et al. [20] reported that more than 40% of cases predicted to be resectable by CT were not resectable during surgical laparotomy because of small metastases in the liver and peritoneal dissemination lesions missed in most cases. From this point of view, the combination of CTAP + CTHA is well suited for the preoperative evaluation of the existence of liver metastases from pancreatic cancer.

US is a noninvasive and relatively inexpensive examination for the detection of liver metastases. However, the sensitivity of US for detecting small metastases (<1 cm) is difficult to establish [21].

Superparamagnetic iron oxide (SPIO)-enhanced MRI has not only improved tumor detection but has also allowed characterization of liver lesions [22]. Strotzer et al. [22] reported that spiral CTAP could not be replaced by SPIO-enhanced MRI because CTAP has higher sensitivity, although its specificity is relatively low. Vogl et al. [23] and Bhattacharjya et al. [15] have reported that the diagnostic efficacy of SPIO-enhanced MRI is similar to that of CTAP. Tanimoto et al. [16] have also reported that the diagnostic efficacy of SPIO-enhanced MRI is similar to that of CTAP + CTHA. In the present study, MRI was not performed for the patients, so we could not compare MRI with MDCT and CTAP + CTHA.

Recently, gadolinium-ethoxybenzyl-diethylenetriamine pentaacetic acid-enhanced magnetic resonance imaging (Gd-EOB-DTPA-MRI) has been shown to be a useful modality for detecting liver tumors [24–27]. Akai et al. [24] have reported that Gd-EOB-DTPA-MRI is as useful as MDCT for detecting liver lesions. Hammerstingl et al. [25] have reported that Gd-EOB-DTPA-MRI is superior for the diagnosis of focal liver lesions compared with MDCT. Recent multicenter studies have reported that Gd-EOB-DTPA-MRI is of clinical benefit relative to unenhanced MRI and spiral CT [26, 27]. However, the majority of the patients in these reports had hepatocellular carcinoma (HCC). Therefore, further studies are needed to compare CTAP + CTHA with Gd-EOB-DTPA-MRI for the detection of liver metastases.

In conclusion, the combination of CTAP and CTHA is useful for the detection of liver metastases before operation for resectable pancreatic cancer because it has higher sensitivity for this purpose than MDCT.

References

1. Kern S, Hruban R, Hollingsworth MA, Brand R, Adrian TE, Jaffee E, et al. The product of a pancreas cancer think tank. Cancer Res. 2001;61:4923–32.
2. Li D, Xie K, Wolff R, Abbruzzese JL. Pancreatic cancer. Lancet. 2004;363:1049–57.
3. Baumel H, Huguier M, Manderscheid JC, Fabre JM, Houry S, Fagot H. Results of resection for cancer of the exocrine pancreas: a study from the French association of surgery. Br J Surg. 1994;81:102–7.
4. Sohn TA, Yeo CJ, Cameron JL, Koniaris L, Kaushal S, Abrams RA, et al. Resected adenocarcinoma of the pancreas—616 patients: results, outcomes, and prognostic indicators. J Gastrointest Surg. 2000;4:567–79.
5. Richter A, Niedergethmann M, Sturm JW, Lorenz D, Post S, Trede M. Long-term results of partial pancreaticoduodenectomy

for ductal adenocarcinoma of the pancreatic head: 25-year experience. World J Surg. 2003;27:324–9.
6. Dalton RR, Sarr MG, van Heerden JA, Colby TV. Carcinoma of the body and tail of the pancreas: is curative resection justified? Surgery. 1992;111:489–94.
7. Brennan MF, Moccia RD, Klimstra D. Management of adenocarcinoma of the body and tail of the pancreas. Ann Surg. 1996;223:506–11. (discussion 511–502).
8. Griffin JF, Smalley SR, Jewell W, Paradelo JC, Reymond RD, Hassanein RE, et al. Patterns of failure after curative resection of pancreatic carcinoma. Cancer. 1990;66:56–61.
9. Sperti C, Pasquali C, Piccoli A, Pedrazzoli S. Recurrence after resection for ductal adenocarcinoma of the pancreas. World J Surg. 1997;21:195–200.
10. Takamori H, Ikeda O, Kanemitsu K, Tsuji T, Chikamoto A, Kusano S, et al. Preoperative detection of liver metastases secondary to pancreatic cancer: utility of combined helical computed tomography during arterial portography with biphasic computed tomography-assisted hepatic arteriography. Pancreas. 2004;29:188–92.
11. Soyer P, Bluemke DA, Hruban RH, Sitzmann JV, Fishman EK. Hepatic metastases from colorectal cancer: detection and false-positive findings with helical CT during arterial portography. Radiology. 1994;193:71–4.
12. Li L, Wu PH, Mo YX, Lin HG, Zheng L, Li JQ, et al. CT arterial portography and CT hepatic arteriography in detection of micro liver cancer. World J Gastroenterol. 1999;5:225–7.
13. Inaba Y, Arai Y, Kanematsu M, Takeuchi Y, Matsueda K, Yasui K, et al. Revealing hepatic metastases from colorectal cancer: value of combined helical CT during arterial portography and CT hepatic arteriography with a unified CT and angiography system. AJR Am J Roentgenol. 2000;174:955–61.
14. Furukawa H, Iwata R, Moriyama N. Is CT during arterial portography useful for the preoperative evaluation of liver metastases from pancreatic carcinoma? Pancreas. 2001;22:200–2.
15. Bhattacharjya S, Bhattacharjya T, Baber S, Tibballs JM, Watkinson AF, Davidson BR. Prospective study of contrast-enhanced computed tomography, computed tomography during arterioportography, and magnetic resonance imaging for staging colorectal liver metastases for liver resection. Br J Surg. 2004;91:1361–9.
16. Tanimoto A, Wakabayashi G, Shinmoto H, Nakatsuka S, Okuda S, Kuribayashi S. Superparamagnetic iron oxide-enhanced MR imaging for focal hepatic lesions: a comparison with CT during arterioportography plus CT during hepatic arteriography. J Gastroenterol. 2005;40:371–80.
17. Matsuo M, Kanematsu M, Inaba Y, Matsueda K, Yamagami T, Kondo H, et al. Pre-operative detection of malignant hepatic tumours: value of combined helical CT during arterial portography and biphasic CT during hepatic arteriography. Clin Radiol. 2001;56:138–45.
18. Satoi S, Yamamoto H, Takai S, Tanigawa N, Komemushi A, Yanagimoto H, et al. Clinical impact of multidetector row computed tomography on patients with pancreatic cancer. Pancreas. 2007;34:175–9.
19. Takamori H, Kanemitsu K, Tsuji T, Tanaka H, Chikamoto A, Nakahara O, et al. 5-Fluorouracil intra-arterial infusion combined with systemic gemcitabine for unresectable pancreatic cancer. Pancreas. 2005;30:223–6.
20. Jimenez RE, Warshaw AL, Rattner DW, Willett CG, McGrath D, Fernandez-del Castillo C. Impact of laparoscopic staging in the treatment of pancreatic cancer. Arch Surg. 2000;135:409–14. (discussion 414–405).
21. Robinson PJ. Imaging liver metastases: current limitations and future prospects. Br J Radiol. 2000;73:234–41.
22. Strotzer M, Gmeinwieser J, Schmidt J, Fellner C, Seitz J, Albrich H, et al. Diagnosis of liver metastases from colorectal adenocarcinoma. Comparison of spiral-CTAP combined with intravenous contrast-enhanced spiral-CT and SPIO-enhanced MR combined with plain MR imaging. Acta Radiol. 1997;38:986–92.
23. Vogl TJ, Schwarz W, Blume S, Pietsch M, Shamsi K, Franz M, et al. Preoperative evaluation of malignant liver tumors: comparison of unenhanced and SPIO (resovist)-enhanced MR imaging with biphasic CTAP and intraoperative US. Eur Radiol. 2003;13:262–72.
24. Akai H, Kiryu S, Takao H, Tajima T, Shibahara J, Imamura H, et al. Efficacy of double-arterial phase gadolinium ethoxybenzyl diethylenetriamine pentaacetic acid-enhanced liver magnetic resonance imaging compared with double-arterial phase multidetector row helical computed tomography. J Comput Assist Tomogr. 2009;33:887–92.
25. Hammerstingl R, Huppertz A, Breuer J, Balzer T, Blakeborough A, Carter R, et al. Diagnostic efficacy of gadoxetic acid (Primovist)-enhanced MRI and spiral CT for a therapeutic strategy: comparison with intraoperative and histopathologic findings in focal liver lesions. Eur Radiol. 2008;18:457–67.
26. Ichikawa T, Saito K, Yoshioka N, Tanimoto A, Gokan T, Takehara Y, et al. Detection and characterization of focal liver lesions: a Japanese phase III, multicenter comparison between gadoxetic acid disodium-enhanced magnetic resonance imaging and contrast-enhanced computed tomography predominantly in patients with hepatocellular carcinoma and chronic liver disease. Invest Radiol. 2010;45:133–41.
27. Raman SS, Leary C, Bluemke DA, Amendola M, Sahani D, McTavish JD et al (2010) Improved characterization of focal liver lesions with liver-specific gadoxetic acid disodium-enhanced magnetic resonance imaging: a multicenter phase 3 clinical trial. J Comput Assist Tomogr 34:163–172.